Journal of
Mechanics of
Materials and Structures

GEOMETRICALLY NONLINEAR EFFECTS IN THE FLEXURAL RESPONSE OF MASONRY WALLS STRENGTHENED WITH COMPOSITE MATERIALS

Ehab Hamed and Oded Rabinovitch

Volume 2, Nº 5 May 2007

mathematical sciences publishers

JOURNAL OF MECHANICS OF MATERIALS AND STRUCTURES
Vol. 2, No. 5, 2007

GEOMETRICALLY NONLINEAR EFFECTS IN THE FLEXURAL RESPONSE OF MASONRY WALLS STRENGTHENED WITH COMPOSITE MATERIALS

EHAB HAMED AND ODED RABINOVITCH

The geometrically nonlinear effects in the out-of-plane flexural response of unreinforced masonry walls strengthened with externally bonded composite materials are analytically investigated. The investigation aims to explore the stabilizing or destabilizing influence of the arching action formed under realistic supporting conditions (restricted longitudinal deformations) of the wall, and to quantify the contribution of the strengthening system to improving the stability characteristics of the wall. The localized buckling effects associated with the development of compressive stresses in the FRP strip are also examined. Variational principles, large displacements kinematics, compatibility conditions between the structural components (masonry units, mortar joints, FRP strips, and adhesive layers), and the assumption of one-way flexural action are used for the formulation of the nonlinear analytical model. The cracking of the mortar joints, which is essential to the development of the arching action, and the formation of debonded zones are also considered. A numerical example that highlights the geometrically nonlinear effects in the response of the strengthened wall and examines the influence of the slenderness ratio is presented. The results quantify the potential increase of the limit point load and deflection due to the externally bonded composite system. They also quantitatively reveal the wrinkling phenomenon of the compressed FRP strip and the shear and peeling stress concentrations that develop in the vicinity of the cracked mortar joints, the debonded regions, and the wrinkled FRP layer. The paper closes with concluding remarks.

Introduction

Unreinforced masonry structures are found in almost every modern or historic building environment all over the world. With the advantages of this classical building technique, come critical deficiencies, namely the vulnerability of masonry structures to lateral (out-of-plane) loads, and especially to wind and seismic loads. This deficiency may result in considerable damage to the masonry structure, loss of functionality, or even injury to the occupants.

Many strengthening and upgrading techniques have been proposed in attempt to improve the strength and stability of unreinforced masonry (URM) walls. Recently, the use of externally bonded composite materials in the form of fiber reinforced polymer (FRP) laminates and fabrics has gained widespread acceptance. The behavior of URM walls strengthened with composite materials and subjected to out-of-plane loading was examined in many experimental studies [Gilstrap and Dolan 1998; Velazquez-Dimas et al. 2000; Albert et al. 2001; Hamilton and Dolan 2001; Hamoush et al. 2002; Kiss et al. 2002; Kuzik et al. 2003; Ghobarah and El Mandooh Galal 2004; Tan and Patoary 2004]. These studies reveal that the use of the externally bonded FRP system leads to an increase of 10–50 times the strength of the masonry

Keywords: arching, buckling, composite materials, cracking, debonding, masonry, nonlinear analysis, strengthening, wrinkling.

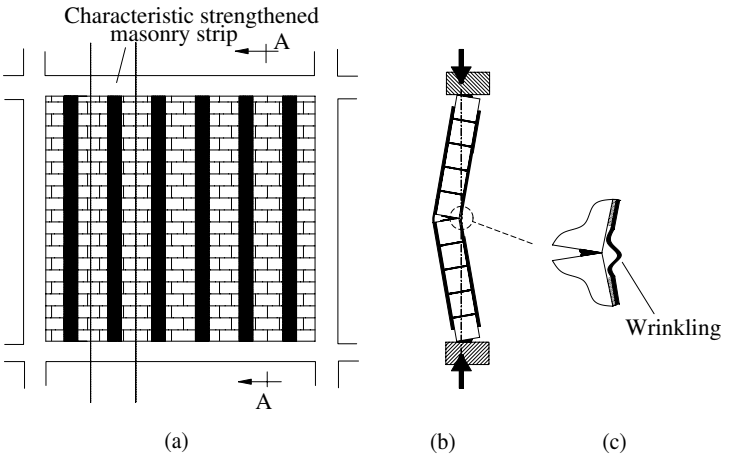

Figure 1. Out-of-plane flexural response of strengthened masonry walls: (a) a one-way strengthening system of FRP strips; (b) section A-A: formation of arching action; (c) localized wrinkling.

wall. However, the majority of the experimental studies focused on ideal boundary conditions, in which the masonry wall is simply supported with no restraint of its in-plane longitudinal deformations.

In practice, masonry walls are usually built within a surrounding frame that restrains the in-plane deformations of the wall's edges (see Figure 1a). These types of supporting conditions, along with the cracking pattern of the wall, lead to the development of eccentric membrane thrust forces and to the formation of the *arching action* (see Figure 1b) [McDowell et al. 1956; Anderson 1984; Dafnis et al. 2002; Griffith et al. 2004]. Under relatively low levels of lateral load (yet beyond the cracking point), the thrust forces increase the compressive stresses in the masonry wall, restraining the cracking in the joints, and forming an eccentric force couple that balances the external bending moment. In this sense the arching action has a stabilizing or strengthening effect on the behavior of the wall. Under higher levels of load, and particularly for slender walls, the geometric nonlinear effect of the compressive forces has a destabilizing effect that may lead to loss of stability and total collapse of the wall. Hence, in the common case of longitudinally constrained masonry walls, and especially for slender walls, the analysis must account for the geometrically nonlinear effects associated with the arching action (see the British standard BS5628 and [Hasetline and Moore 1981]).

The restriction of the longitudinal deformations and the formation of the thrust forces may induce compressive stresses in the externally bonded FRP reinforcement, along with the global geometrically nonlinear effects. These forces may trigger localized geometrically nonlinear effects in the form of localized buckling or wrinkling of the FRP layer (see Figure 1c and [Rabinovitch 2004b; [UBC 1991, pp. 227–232]; Deuring 1993]). Hence, the analysis of the strengthened wall must also account for the geometrically nonlinear effects on the localized scale.

A comparatively small number of research projects focus on the out-of-plane behavior of strengthened walls with realistically constrained edges, in contrast to the vast amount of research on unconstrained

masonry walls strengthened with composite materials. [Tumialan et al. 2000; Tumialan et al. 2003] presented results of field tests conducted on existing URM walls. These studies showed that the capacity of the strengthened wall is only about 1.4 times higher than the unstrengthened one. This strengthening ratio is much smaller than the ones obtained using ideal, simply supported and longitudinally unconstrained edges. Based on experimental observations, [Galati et al. 2002] indicated that strengthened URM walls, with longitudinally constrained edges, may undergo two failure mechanisms that include flexural failure (masonry crushing and FRP rupture) or shear-compression failure at the supports. The latter mode is directly attributed to the formation of the arching thrust forces. The experimental study of [Davidson et al. 2005] focused on the behavior of strengthened URM walls subjected to blast loadings. It was found that the wall-frame gap, and thus the level of development of the arching action, affects the behavior of the wall and its failure mechanisms.

In terms of theoretical models, [Tumialan et al. 2003] proposed a linear model for the evaluation of the peak load and deflection of strengthened URM walls subjected to out-of-plane loading. This model considers cracking of the mortar joints at midspan and at the supports only, and is based on the displacement pattern of three hinged rigid bodies. At the section level, the strain compatibility approach was adopted. This geometrically linear model provides an acceptable prediction of the ultimate load in cases of crushing failure of the masonry units under relatively low levels of load. However, the consideration of the geometrically nonlinear destabilizing effects of the arching action and the consideration of the wrinkling and buckling of the compressed FRP strip near the mortar joints are beyond the scope of this model. [Davidson et al. 2005] used nonlinear FE models for the analysis of strengthened masonry walls subjected to blast loadings. This type of analysis accounts for the stability aspects. However, the different length scales (thickness of the adhesive layer and the FRP strip with respect to the thickness of the masonry unit), the differences in the mechanical properties of the materials, and the singularities and stress concentrations at critical points, make the application of the FE method for the nonlinear analysis of strengthened masonry walls computational effort consuming.

In this paper, the global and local geometrically nonlinear effects are investigated. The objectives of this paper are to gain insight into the geometrically nonlinear effects in the out-of-plane flexural response of URM walls strengthened with composite materials, and to provide a theoretical approach for the nonlinear analysis of the strengthened wall. In particular, the paper focuses on exploring and quantifying the stabilizing/destabilizing influence of the arching effect; the contribution of the strengthening system to the improvement of the stability characteristics of the wall; and the localized buckling/wrinkling of the compressed FRP strip near the mortar joints. The analytical model assumes a one-way flexural response of the strengthened wall. Although in some cases two-way out-of-plane flexural action is possible, in most practical cases, the boundary conditions of the existing wall (which usually consist of only two opposite supported edges) and the use of strengthening system with one-way FRP strips (which is generally easier to install) yield an overall one-way action of the strengthened wall [Davidson et al. 2005]. It is also assumed that the stress and deformation fields are uniform through the width of the FRP strips and the adhesive layers, as well as through the active width of the masonry strip, as seen in Figure 1a,b [Davidson et al. 2005; Hamilton and Dolan 2001].

The geometrically nonlinear effects are considered through the large displacements, moderate rotations, and small strain kinematic relations. Variational principles, static equilibrium, and compatibility requirements between the masonry units, mortar joints, FRP strips, and the adhesive layers, are also

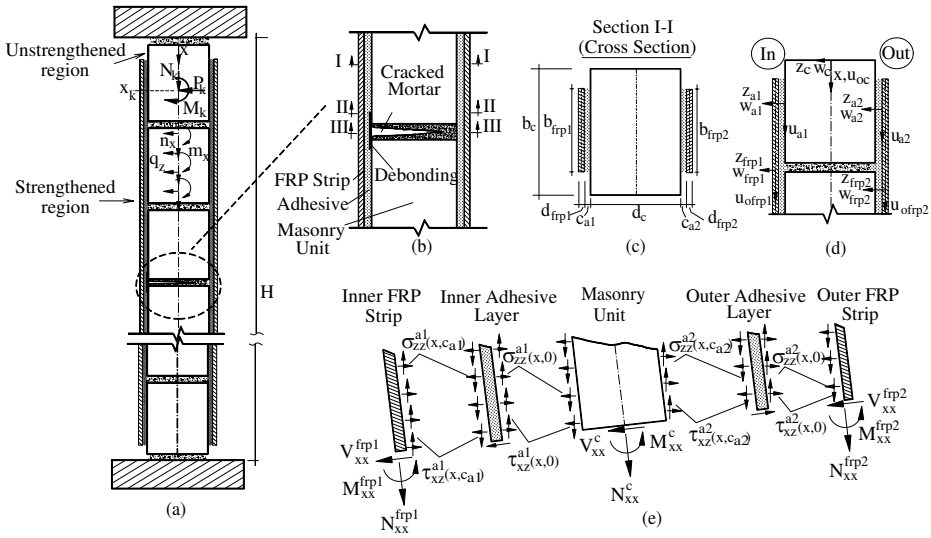

Figure 2. Geometry, loads, sign conventions, and stress resultants: (a) geometry and loads; (b) cracked mortar joint and debonded regions; (c) section I-I (cross section); (d) coordinate systems and deformations; (e) stresses and stress resultants.

used in the derivation of the analytical model. The material behavior of the masonry units, the FRP strips, and the adhesive material is assumed to be linear elastic, whereas the constitutive model for the mortar joints accounts for their brittle cracking behavior. Compatibility and continuity conditions are used for the assembly of the various components of the wall into a whole structure. Perfect bonding and the ability to transfer shear and normal stresses are assumed at the interfaces between the various components. Yet, the formation of debonded regions, in which the adhesive-mortar interface cannot transfer shear stresses, is considered in case the mortar joint is cracked, or in case the masonry-mortar interface is partially detached [Hamilton and Dolan 2001; Albert et al. 2001]. Finally, it is assumed that the debonded regions do not grow under loading.

The mathematical formulation of the nonlinear analytical model is presented next. It is followed by a numerical example and a comparison of the theoretical results with finite element analyses. Finally, concluding remarks are presented.

Mathematical formulation

The strengthened masonry wall is shown in Figure 1 and the sign conventions for the coordinates, deformations, loads, stresses, and stress resultants are shown in Figure 2. Note that, due to the one-way action of the strengthening system, the formulation focuses on a characteristic masonry strip. The masonry units and the mortar joints are modeled using the first order shear deformation theory (*Timoshenko's beams*, [Timoshenko and Goodier 1970]). The FRP strips are modeled using the lamination and the first order shear deformation theories, and the adhesive layers are modeled as 2D linear elastic continua with shear and out-of-plane normal rigidities only [Rabinovitch and Frostig 2000]. In the masonry unit section, the longitudinal rigidity of the adhesive layers is neglected, due to its minor contribution to the overall

flexural rigidity of the strengthened section. In the mortar joint section, the increased longitudinal strains that develop in the FRP strips bridging over the cracked mortar joint result in a failure of the adhesive material that may still be attached to the debonded FRP strip. Thus, the longitudinal rigidity of the adhesive is neglected in this region as well.

Figure 2a shows that the strengthened strip may consist of regions strengthened on two sides and regions that are not strengthened through the height of the wall. In other cases, strengthening on one side of the wall may also be considered. For the sake of generality, the formulation presented next focuses on walls externally strengthened on both sides. Figure 2b shows that the two-side strengthened region may include two types of subregions. The first one is a *fully bonded* sub-region in which the FRP strip is firmly attached through the adhesive layer (section I-I in Figure 2b). The second sub-region is a debonded one in which one of the interfaces loses its ability to transfer shear stresses (sections II-II and III-III in Figure 2b). Such debonded regions may result from improper fastening of the bonded system, unleveled faces of the masonry wall, gaps near the mortar joints, or, most likely, from cracking of the mortar joints. While the debonded interface cannot resist shear stresses, it can transfer out-of-plane normal compressive stresses where contact exists. Hence, the model further distinguishes between debonded subregions with contact and debonded subregions without contact.

The field equations and the boundary/continuity conditions for the fully bonded region and for the two types of debonded subregions are derived using the variational principle of virtual work:

$$\delta(U+V)=0; \tag{1}$$

where U is the strain energy, V is the potential of the external loads, and δ is the variational operator. The first variation of the strain energy is

$$\begin{aligned}\delta U = &\sum_{1}^{N_{\mathrm{mu}}}\int_{V_{\mathrm{mu}}}\left(\sigma_{xx}^{\mathrm{mu}}\delta\varepsilon_{xx}^{\mathrm{mu}}+\tau_{xz}^{\mathrm{mu}}\delta\gamma_{xz}^{\mathrm{mu}}\right)dv_{\mathrm{mu}}+\sum_{1}^{N_{\mathrm{mj}}}\int_{V_{\mathrm{mj}}}\left(\sigma_{xx}^{\mathrm{mj}}\delta\varepsilon_{xx}^{\mathrm{mj}}+\tau_{xz}^{\mathrm{mj}}\delta\gamma_{xz}^{\mathrm{mj}}\right)dv_{\mathrm{mj}}\\ &+\int_{V_{\mathrm{frp1}}}\left(\sigma_{xx}^{\mathrm{frp1}}\delta\varepsilon_{xx}^{\mathrm{frp1}}+\tau_{xz}^{\mathrm{frp1}}\delta\gamma_{xz}^{\mathrm{frp1}}\right)dv_{\mathrm{frp1}}+\int_{V_{\mathrm{frp2}}}\left(\sigma_{xx}^{\mathrm{frp2}}\delta\varepsilon_{xx}^{\mathrm{frp2}}+\tau_{xz}^{\mathrm{frp2}}\delta\gamma_{xz}^{\mathrm{frp2}}\right)dv_{\mathrm{frp2}}\\ &+\int_{V_{\mathrm{a1}}}\left(\tau_{xz}^{\mathrm{a1}}\delta\gamma_{xz}^{\mathrm{a1}}+\sigma_{zz}^{\mathrm{a1}}\delta\varepsilon_{zz}^{\mathrm{a1}}\right)dv_{\mathrm{a1}}+\int_{V_{\mathrm{a2}}}\left(\tau_{xz}^{\mathrm{a2}}\delta\gamma_{xz}^{\mathrm{a2}}+\sigma_{zz}^{\mathrm{a2}}\delta\varepsilon_{zz}^{\mathrm{a2}}\right)dv_{\mathrm{a2}};\end{aligned} \tag{2}$$

where the notations 'mu', 'mj', 'frp1', 'frp2', 'a1' and 'a2' refer to the masonry unit, mortar, inner FRP strip, outer FRP strip, inner adhesive layer, and the outer adhesive layer, respectively; σ_{xx}^{i} and ε_{xx}^{i} are the in-plane normal stress and strain in the masonry unit ($i=\mathrm{mu}$), the mortar joint ($i=\mathrm{mj}$), and the FRP strips ($i=\mathrm{frp1}$ or $i=\mathrm{frp2}$); τ_{xz}^{i} and γ_{xz}^{i} ($i=\mathrm{mu}, \mathrm{mj}, \mathrm{frp1}, \mathrm{frp2}$) are the shear stress and shear angle in the masonry unit, the mortar joint, the FRP strips, respectively; σ_{zz}^{aj} and ε_{zz}^{aj} ($j=1,2$) are the out-of-plane normal stresses and strains in the inner and the outer adhesive layers, respectively; τ_{xz}^{aj} and γ_{xz}^{aj} ($j=1,2$) are the shear stress and shear angle in the adhesive layers; and N_{mu} and N_{mj} are the number of the masonry units and the mortar joints, respectively.

The nonlinear kinematic relations for the masonry units, the mortar joints, and the FRP strips follow the first order shear deformation theory and the assumption of large displacements, moderate rotations,

and small strains as follows:

$$w_i(x, z_i) = w_i(x); \tag{3a}$$

$$u_i(x, z_i) = u_{oi}(x) - z_i\phi_i(x); \tag{3b}$$

$$\gamma^i_{xz}(x, z_i) = w_{i,x}(x) - \phi_i(x); \tag{3c}$$

$$\varepsilon^i_{xx}(x, z_i) = u_{oi,x}(x) + \frac{1}{2}(w_{i,x}(x))^2 - z_i\phi_{i,x}(x); \tag{3d}$$

where $w_i(x)$, $u_{oi}(x)$ and $\phi_i(x)$ are the out-of-plane displacement, the in-plane displacement, and the rotation of the reference line of the masonry unit ($i = \text{mu}$), the mortar joint ($i = \text{mj}$), and the FRP strips ($i = \text{frp1}, \text{frp2}$), respectively, z_i is measured from the reference line of each component inwards (the reference lines are arbitrarily located at the middle plane of each component, see Figure 2d), and $(\,)_{,x}$ denotes a derivative with respect to x. Since both the masonry units and the mortar joints are modeled using the same kinematic assumptions and differ in their constitutive model only, the superscripts mu and mj are replaced with c. Thus, $c = \text{mu}$ refers to the masonry unit regions (sections I-I and II-II in Figure 2b), and $c = \text{mj}$ refers to the mortar regions (section III-III in Figure 2b).

The kinematic relations for the adhesive are:

$$\varepsilon^{aj}_{zz}(x, z_{aj}) = w_{aj,z}(x, z_{aj}); \tag{4a}$$

$$\gamma^{aj}_{xz}(x, z_{aj}) = u_{aj,z}(x, z_{aj}) + w_{aj,x}(x, z_{aj}) \qquad (j = 1, 2); \tag{4b}$$

where w_{aj} and u_{aj} are the out-of-plane and in-plane displacements of the inner ($j = 1$) and outer ($j = 2$) adhesive layers, respectively.

The loads are exerted at the masonry wall only. Thus, the first variation of the potential of the external loads equals:

$$\delta V = -\int_{x=0}^{x=H} (q_z\delta w_c + n_x\delta u_{oc} + m_y\delta\phi_c)\,dx - \sum_{k=1}^{NC}\int_{x=0}^{x=H} \big(P_k\delta w_c(x_k) + N_k\delta u_{oc}(x_k) + M_k\delta\phi_c(x_k)\big)\delta_D(x - x_k)dx; \tag{5}$$

where q_z, n_x, and m_y are distributed loads and bending moments, respectively, P_k, N_k, and M_k are concentrated loads and bending moments at $x = x_k$ (see Figure 2a), δ_D is the Dirac function, and NC is the number of the concentrated loads and moments.

Compatibility and debonding conditions. In the fully bonded subregions, the compatibility conditions at the adhesive-masonry, adhesive-mortar, and adhesive-FRP interfaces read:

$$w_{\text{a1}}(x, z_{\text{a1}} = 0) = w_c(x); \tag{6a}$$

$$u_{\text{a1}}(x, z_{\text{a1}} = 0) = u_{oc}(x) - \frac{d_c}{2}\phi_c(x); \tag{6b}$$

$$w_{\mathrm{a1}}(x, z_{\mathrm{a1}} = c_{\mathrm{a1}}) = w_{\mathrm{frp1}}(x); \tag{7a}$$

$$u_{\mathrm{a1}}(x, z_{\mathrm{a1}} = c_{\mathrm{a1}}) = u_{o\,\mathrm{frp1}}(x) + \frac{d_{\mathrm{frp1}}}{2}\phi_{\mathrm{frp1}}(x); \tag{7b}$$

$$w_{\mathrm{a2}}(x, z_{\mathrm{a2}} = 0) = w_{\mathrm{frp2}}(x); \tag{8a}$$

$$u_{\mathrm{a2}}(x, z_{\mathrm{a2}} = 0) = u_{o\,\mathrm{frp2}}(x) - \frac{d_{\mathrm{frp2}}}{2}\phi_{\mathrm{frp2}}(x); \tag{8b}$$

$$w_{\mathrm{a2}}(x, z_{\mathrm{a2}} = c_{\mathrm{a2}}) = w_c(x); \tag{9a}$$

$$u_{\mathrm{a2}}(x, z_{\mathrm{a2}} = c_{\mathrm{a2}}) = u_{oc}(x) + \frac{d_c}{2}\phi_c(x); \tag{9b}$$

where $d_c (= d_{\mathrm{mu}}$ or $d_{\mathrm{mj}})$, d_{frp1} and d_{frp2} are the thicknesses of the masonry unit, the mortar joint, and the FRP strips, respectively; c_{a1} and c_{a2} are the thicknesses of the inner and outer adhesive layers, respectively; and $z_{aj} (j = 1, 2)$ are measured from the outer interface of each adhesive layer inwards; see Figure 2d.

In the debonded subregions, the interfaces are free of shear and may slip with respect to each other. Hence, the condition of compatible longitudinal deformations is replaced with the condition of shear free interface. For example, in case the inner adhesive-masonry interface is debonded, Equation (6b) is replaced with:

$$\tau^{\mathrm{a1}}_{xz}(x, z_{\mathrm{a1}} = 0) = 0. \tag{10}$$

If the debonded interfaces are in contact, the condition of compatible out-of-plane deformations holds. If out-of-plane contact does not exist, the compatibility condition is replaced with the null normal stress condition. In the case mentioned above, Equation (6a) is replaced with:

$$\sigma^{\mathrm{a1}}_{zz}(x, z_{\mathrm{a1}} = 0) = 0. \tag{11}$$

Nonlinear field equations. The nonlinear field (equilibrium) equations for the strengthened (bonded or debonded) regions are formulated using the variational principle (Equations (1), (2), (5)), along with the kinematic relations (Equations (3a)a–d, (4)) and the compatibility requirements (Equations (6)–(11)). The field equations take the following form:

$$N^{\mathrm{frp1}}_{xx,x}(x) - \alpha_1^{frp} b_{\mathrm{frp1}} \tau^{\mathrm{a1}}_{xz}(x, z_{\mathrm{a1}} = c_{\mathrm{a1}}) = 0; \tag{12}$$

$$N^{c}_{xx,x}(x) - \alpha_2^{c} b_{\mathrm{frp2}} \tau^{\mathrm{a2}}_{xz}(x, z_{\mathrm{a2}} = c_{\mathrm{a2}}) + \alpha_1^{c} b_{\mathrm{frp1}} \tau^{\mathrm{a1}}_{xz}(x, z_{\mathrm{a1}} = 0) = -n_x(x); \tag{13}$$

$$N^{\mathrm{frp2}}_{xx,x}(x) + \alpha_2^{frp} b_{\mathrm{frp2}} \tau^{\mathrm{a2}}_{xz}(x, z_{\mathrm{a2}} = 0) = 0; \tag{14}$$

$$V^{\mathrm{frp1}}_{xz,x}(x) + \left(N^{\mathrm{frp1}}_{xx}(x) w_{\mathrm{frp1},x}(x)\right)_{,x} - \beta_1^{frp} b_{\mathrm{frp1}} \sigma^{\mathrm{a1}}_{zz}(x, z_{\mathrm{a1}} = c_{\mathrm{a1}}) = 0; \tag{15}$$

$$V^{c}_{xz,x}(x) + \left(N^{c}_{xx}(x) w_{c,x}(x)\right)_{,x} + \beta_1^{c} b_{\mathrm{frp1}} \sigma^{\mathrm{a1}}_{zz}(x, z_{\mathrm{a1}} = 0) - \beta_2^{c} b_{\mathrm{frp2}} \sigma^{\mathrm{a2}}_{zz}(x, z_{\mathrm{a2}} = c_{\mathrm{a2}}) = -q_z(x); \tag{16}$$

$$V^{\text{frp2}}_{xz,x}(x) + \left(N^{\text{frp2}}_{xx}(x) w_{\text{frp2},x}(x)\right)_{,x} + \beta_2^{frp} b_{\text{frp2}} \sigma^{\text{a2}}_{zz}(x, z_{\text{a2}} = 0) = 0; \tag{17}$$

$$M^{\text{frp1}}_{xx,x}(x) - V^{\text{frp1}}_{xz}(x) + \alpha_1^{frp} b_{\text{frp1}} \frac{d_{\text{frp1}}}{2} \tau^{\text{a1}}_{xz}(x, z_{\text{a1}} = c_{\text{a1}}) = 0; \tag{18}$$

$$M^{c}_{xx,x}(x) - V^{c}_{xz}(x) + \alpha_1^{c} b_{\text{frp1}} \frac{d_c}{2} \tau^{\text{a1}}_{xz}(x, z_{\text{a1}} = 0) + \alpha_2^{c} b_{\text{frp2}} \frac{d_c}{2} \tau^{\text{a2}}_{xz}(x, z_{\text{a2}} = c_{\text{a2}}) = m_y(x); \tag{19}$$

$$M^{\text{frp2}}_{xx,x}(x) - V^{\text{frp2}}_{xz}(x) + \alpha_2^{frp} b_{\text{frp2}} \frac{d_{\text{frp2}}}{2} \tau^{\text{a2}}_{xz}(x, z_{\text{a2}} = 0) = 0; \tag{20}$$

$$\tau^{\text{a1}}_{xz,x}(x, z_{\text{a1}}) + \sigma^{\text{a1}}_{zz,z}(x, z_{\text{a1}}) = 0; \tag{21}$$

$$\tau^{\text{a1}}_{xz,z}(x, z_{\text{a1}}) = 0; \tag{22}$$

$$\tau^{\text{a2}}_{xz,x}(x, z_{\text{a2}}) + \sigma^{\text{a2}}_{zz,z}(x, z_{\text{a2}}) = 0; \tag{23}$$

$$\tau^{\text{a2}}_{xz,z}(x, z_{\text{a2}}) = 0; \tag{24}$$

where N^i_{xx}, V^i_{xz}, and M^i_{xx} ($i = c, \text{frp1}, \text{frp2}$) are the in-plane, shear, and the bending moment stress resultants, respectively, in the masonry unit, the mortar joint, and the FRP strips; b_i ($i = \text{frp1}, \text{frp2}$) is the width of the inner and outer FRP strips; α^n_m is a flag that equals 0 for a debonded interface or equals 1 for a bonded one ($m = 1$ for the inner adhesive layer and $m = 2$ for the outer adhesive layer; $n = frp$ for the adhesive-FRP interface and $n = c$ for the adhesive-masonry/mortar interface, see Figure 2d); β^n_m is also a flag that equals 0 for debonding without contact or equals 1 for debonding with contact, with the above notation for m and n. Note that Equations (12)–(24) are valid for both the masonry regions ($c = \text{mu}$) and the mortar regions ($c = \text{mj}$), whereas the distinction between the two cases is achieved through the constitutive relations.

Boundary and continuity conditions. The boundary conditions at the edges of the masonry panel and the FRP strips are:

$$\psi N^i_{xx} = \vartheta N_k \qquad \text{or} \qquad u_{oi} = \bar{u}_{oi}; \tag{25}$$

$$-\psi M^i_{xx} = \vartheta M_k \qquad \text{or} \qquad \phi_i = \bar{\phi}_i; \tag{26}$$

$$\psi (V^i_{xz} + N^i_{xx} w_{i,x}) = \vartheta P_k \qquad \text{or} \qquad w_i = \bar{w}_i; \tag{27}$$

where P_k, N_k and M_k are external loads and bending moments at $x_k = 0$ or $x_k = H$; $\bar{u}_{oi}$, $\bar{w}_i$ and $\bar{\phi}_i (i = c, \text{frp1}, \text{frp2})$ are prescribed deformations and rotations; $\psi = 1$ where $x = H$; $\psi = -1$ where $x = 0$; $\vartheta = 1$ for the boundary conditions of the masonry units or the mortar joints; and $\vartheta = 0$ for the boundary conditions of the FRP strips.

The boundary conditions at the edges of the adhesive layers are:

$$\tau^{aj}_{xz}(z_{aj}) = 0 \qquad \text{or} \qquad w_{aj}(z_{aj}) = \bar{w}_{aj}(z_{aj}); \tag{28}$$

where $\bar{w}_{aj}(z_{aj}) (j = 1, 2)$ are prescribed deformation distributions through the thicknesses of the adhesive layers.

The continuity conditions at any point $x = x_k$ within the fully bonded sub-region are $i = c$, frp1, frp2; $j = 1, 2$

$$u_{oi}^{(-)} = u_{oi}^{(+)}; \qquad w_i^{(-)} = w_i^{(+)}; \qquad \phi_i^{(-)} = \phi_i^{(+)}; \tag{29}$$

$$N_{xx}^{i(-)} - N_{xx}^{i(+)} = \vartheta N_k; \qquad -M_{xx}^{i(-)} + M_{xx}^{i(+)} = \vartheta M_k; \tag{30}$$

$$V_{xz}^{i(-)} + N_{xx}^{i(-)} w_{i,x}^{(-)} - V_{xz}^{i(+)} - N_{xx}^{i(+)} w_{i,x}^{(+)} = \vartheta P_k; \tag{31}$$

$$\tau_{xz}^{aj(-)}(z_{aj}) = \tau_{xz}^{aj(+)}(z_{aj}); \qquad w_{aj}^{(-)}(z_{aj}) = w_{aj}^{(+)}(z_{aj}); \tag{32}$$

where the superscripts $(-)$ and $(+)$ denote quantities left and right to the point $x = x_k$, respectively.

Constitutive relations. The cracking of the mortar joints is a critical condition for the development of the arching action. Hence, the analysis must account for this type of physical nonlinear constitutive behavior. Based on the experimental observations of [Velazquez-Dimas et al. 2000] and [Hamilton and Dolan 2001], it is assumed that cracking is limited to the mortar joints. Hence, the constitutive relations for the masonry units assume linear elastic behavior, whereas the constitutive model for the mortar assumes a linear elastic behavior in compression and a brittle cracking behavior in tension. (Note that the constitutive model for the mortar can be extended to include a nonlinear behavior in compression. However, these effects are beyond the scope of this paper and are not considered here). The material point level constitutive relation for the normal stresses in the mortar is:

$$\sigma_{xx}^{\mathrm{mj}} = \begin{Bmatrix} E_{\mathrm{mj}}\varepsilon_{xx}^{\mathrm{mj}}, & \text{if } \varepsilon_{xx}^{\mathrm{mj}} \le \varepsilon_t^{\mathrm{mj}} \\ 0, & \text{if } \varepsilon_{xx}^{\mathrm{mj}} > \varepsilon_t^{\mathrm{mj}} \end{Bmatrix}, \tag{33}$$

where E_{mj} is the modulus of elasticity of the mortar, and $\varepsilon_t^{\mathrm{mj}}$ is its the ultimate tensile or bond strain. The generalized (cross-sectional) constitutive relations for the masonry units and the mortar joints are:

$$N_{xx}^c = \int_{A_c} \sigma_{xx}^c(z_c) dA_c = A_{11}^c \left(u_{oc,x} + \frac{1}{2}(w_{c,x})^2 \right) - B_{11}^c \phi_{c,x} \quad (c = \text{mu or mj}); \tag{34}$$

$$M_{xx}^c = \int_{A_c} \sigma_{xx}^c(z_c) z_c dA_c = B_{11}^c \left(u_{oc,x} + \frac{1}{2}(w_{c,x})^2 \right) - D_{11}^c \phi_{c,x} \quad (c = \text{mu or mj}); \tag{35}$$

$$V_{xx}^c = \int_{A_c} \tau_{xz}^c(z_c) dA_c = A_{55}^c (w_{c,x} - \phi_c) \quad (c = \text{mu or mj}); \tag{36}$$

where A_{11}^c, B_{11}^c, D_{11}^c and A_{55}^c are the extensional, coupling, flexural, and shear rigidities of the masonry unit ($c = \text{mu}$) or the mortar joint ($c = \text{mj}$), multiplied by b_c, which is the width of the examined strengthened masonry strip.

Due to the assumed linear elastic behavior of the masonry unit material, the equivalent rigidities of the masonry units reduce to the traditional extensional, flexural and shear rigidities of the elastic section:

$$A_{11}^{\mathrm{mu}} = \int_{-d_{\mathrm{mu}}/2}^{d_{\mathrm{mu}}/2} b_{\mathrm{mu}} E_{\mathrm{mu}} dz_{\mathrm{mu}} = EA_{\mathrm{mu}}; \tag{37a}$$

$$B_{11}^{\mathrm{mu}} = \int_{-d_{\mathrm{mu}}/2}^{d_{\mathrm{mu}}/2} b_{\mathrm{mu}} E_{\mathrm{mu}} z_{\mathrm{mu}} dz_{\mathrm{mu}} = 0; \tag{37b}$$

$$D_{11}^{\mathrm{mu}} = \int_{-d_{\mathrm{mu}}/2}^{d_{\mathrm{mu}}/2} b_{\mathrm{mu}} E_{\mathrm{mu}} z_{\mathrm{mu}}^2 dz_{\mathrm{mu}} = EI_{\mathrm{mu}}; \tag{37c}$$

$$A_{55}^{\mathrm{mu}} = \int_{-d_{\mathrm{mu}}/2}^{d_{\mathrm{mu}}/2} b_{\mathrm{mu}} G_{\mathrm{mu}} dz_{\mathrm{mu}} = \kappa GA_{\mathrm{mu}}; \tag{37d}$$

where E_{mu} and G_{mu} are the elastic and shear moduli of the masonry unit, EA_{mu}, EI_{mu} and GA_{mu} are the extensional, flexural and shear stiffnesses of the masonry unit section, respectively, $b_{\mathrm{mu}} = b_c$, and κ is the shear correction constant.

In the mortar joint, the nonlinear constitutive law and the combined in-plane and bending tractions require special consideration. The general stress and strain distributions under various combined tractions appear in Figure 3a–c. In case the tensile strains are lower than the ultimate tensile/bond strain $\varepsilon_t^{\mathrm{mj}}$ (Figure 3a), the mortar joint is *uncracked* and it exhibits a linear elastic behavior. Therefore, the equivalent rigidities are given by Equation (37)a–d with the subscript/superscript mj instead of mu. In case the tensile strains exceed $\varepsilon_t^{\mathrm{mj}}$ (Figure 3b), the mortar joint is *cracked* and the equivalent rigidities take the following form:

$$A_{11}^{\mathrm{mj}} = \int_{-d_{\mathrm{mj}}/2}^{z_{act}^{\mathrm{mj}}} b_{\mathrm{mj}} E_{\mathrm{mj}} dz_{\mathrm{mj}} = E_{\mathrm{mj}} b_{\mathrm{mj}} \left(\frac{d_{\mathrm{mj}}}{2} + \varphi z_{act}^{\mathrm{mj}} \right); \tag{38a}$$

$$B_{11}^{\mathrm{mj}} = \int_{-d_{\mathrm{mj}}/2}^{z_{act}^{\mathrm{mj}}} b_{\mathrm{mj}} E_{\mathrm{mj}} z_{\mathrm{mj}} dz_{\mathrm{mj}} = -\varphi \frac{E_{\mathrm{mj}} b_{\mathrm{mj}}}{2} \left(\left(\frac{d_{\mathrm{mj}}}{2} \right)^2 - \left(z_{act}^{\mathrm{mj}} \right)^2 \right); \tag{38b}$$

$$D_{11}^{\mathrm{mj}} = \int_{-d_{\mathrm{mj}}/2}^{z_{act}^{\mathrm{mj}}} b_{\mathrm{mj}} E_{\mathrm{mj}} z_{\mathrm{mj}}^2 dz_{\mathrm{mj}} = \frac{E_{\mathrm{mj}} b_{\mathrm{mj}}}{3} \left(\left(\frac{d_{\mathrm{mj}}}{2} \right)^3 + \varphi \left(z_{act}^{\mathrm{mj}} \right)^3 \right); \tag{38c}$$

$$A_{55}^{\mathrm{mj}} = \int_{-d_{\mathrm{mj}}/2}^{z_{act}^{\mathrm{mj}}} b_{\mathrm{mj}} G_{\mathrm{mj}} dz_{\mathrm{mj}} = \kappa G_{\mathrm{mj}} b_{\mathrm{mj}} \left(\frac{d_{\mathrm{mj}}}{2} + \varphi z_{act}^{\mathrm{mj}} \right); \tag{38d}$$

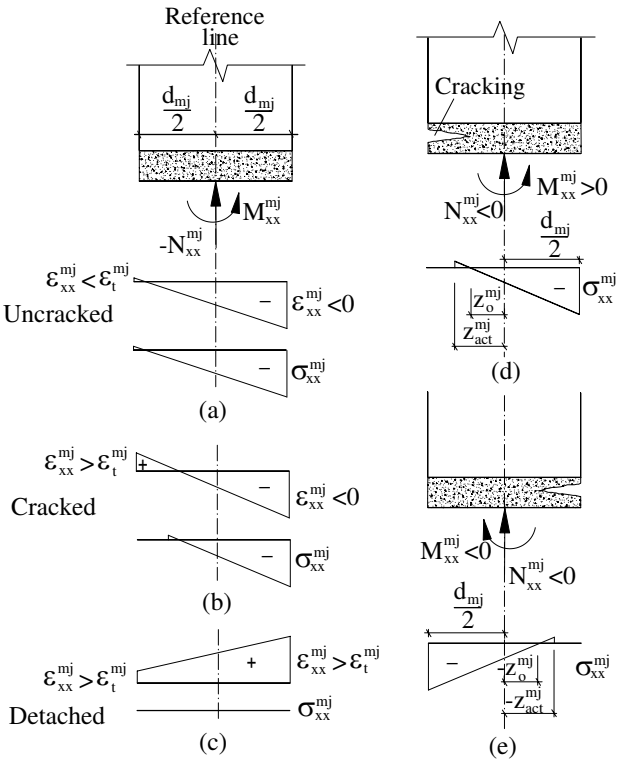

Figure 3. Stress distributions through the mortar joint: (a) uncracked joint; (b) cracked joint; (c) detached joint; (d) stress distribution under positive moment and compressive force; (e) stress distribution under negative moment and compressive force.

where according to Figure 3, b_{mj} and z_{act}^{mj} define the width and the depth of the active zone in the mortar cross section, $\varphi = 1$ in case the mortar section is locally subjected to in-plane compression combined with a positive bending moment (Figure 3d), $\varphi = -1$ if the in-plane compression is combined with a negative bending moment (Figure 3e) and G_{mj} is the shear modulus of the mortar. In case the mortar joint is fully detached (Figure 3c), its rigidities are zero and the functionality of the strengthened wall depends on the FRP strips only. In most practical cases, the contribution of the tensioned mortar to the stiffness of the cracked cross section is negligible, and thus z_{act}^{mj} can be replaced with z_o^{mj}, which is the height of the neutral axis; see Figure 3.

The constitutive relations of the FRP strips follow the classical lamination theory and use Equations (33)–(35) with the superscripts/subscripts frp1 or frp2 instead of c. In this case, A_{11}^i, B_{11}^i, D_{11}^i and $A_{55}^i (i = \mathrm{frp1}, \mathrm{frp2})$ are the extensional, coupling, flexural, and shear rigidities of the inner and outer FRP strips, respectively [Vinson and Sierakowski 1986], multiplied by the width of the strip. Note that the shear rigidity of the FRP strip may be one or two orders of magnitude smaller than its extensional rigidity, which may affect the localized buckling characteristics of the FRP strip [Sheinman and Adan 1987].

The constitutive relations for the adhesive material assume linear-elastic behavior, and read

$$\sigma_{zz}^{aj} = E_{aj}\varepsilon_{zz}^{aj}, \quad \tau_{xz}^{aj} = G_{aj}\gamma_{xz}^{aj}, \qquad (j = 1, 2), \tag{39}$$

where E_{aj} and G_{aj} $(j = 1, 2)$ are the modulus of elasticity and the shear modulus of the adhesive material, respectively. Note that in some cases, the material behavior of the adhesive may exhibit some nonlinear or inelastic characteristics. These effects, and especially their influence on the localized stress concentrations in the adhesive layer in externally strengthened reinforced concrete beams, are studied in [Rabinovitch 2005]. For brevity, and in order to focus on the geometrically nonlinear effects, they are not studied here.

Adhesive layers—stress and displacement fields. The stress and displacement fields of the adhesive layers follow the high-order approach [Rabinovitch and Frostig 2000], and are derived using Equations (21)–(24), along with the compatibility requirements/debonding conditions (Equations (6)–(11)) and the kinematic and constitutive relations (Equations (4), (39)). In the fully bonded regions they take the following form:

$$\tau_{xz}^{aj}(x, z_{aj}) = \tau_{xz}^{aj}(x) = \tau_{aj}; \tag{40}$$

$$\sigma_{zz}^{aj}(x, z_{aj}) = -\frac{2z_{aj} - c_{aj}}{2}\tau_{aj,x} + \frac{\lambda E_{aj}(w_i - w_c)}{c_{aj}}; \tag{41}$$

$$w_{aj}(x, z_{aj}) = -\frac{z_{aj}^2 - c_{aj}z_{aj}}{2E_{aj}}\tau_{aj,x} + \frac{\lambda(w_i - w_c)z_{aj}}{c_{aj}} + \frac{(1+\lambda)}{2}w_c + \frac{(1-\lambda)}{2}w_{\text{frp2}}; \tag{42}$$

$$\begin{aligned} u_{aj}(x, z_{aj}) = {} & \frac{\tau_{aj}z_{aj}}{G_{aj}} + \frac{\tau_{aj,xx}}{2E_{aj}}\left(\frac{z_{aj}^3}{3} - c_{aj}\frac{z_{aj}^2}{2}\right) - \frac{\lambda\left(w_{i,x} - w_{c,x}\right)z_{aj}^2}{2c_{aj}} \\ & - \frac{(\lambda+1)}{2}\left(w_{c,x}z_{\text{a1}} - u_{oc} + \frac{d_c}{2}\phi_c\right) + \frac{(\lambda-1)}{2}\left(w_{\text{frp2},x}z_{\text{a2}} - u_{oc} + \frac{d_{\text{frp2}}}{2}\phi_{\text{frp2}}\right); \end{aligned} \tag{43}$$

where $\lambda = 1$ for $j = 1$ and $i = \text{frp1}$, and $\lambda = -1$ for $j = 2$ and $i = \text{frp2}$. The stress fields in the debonded subregions (with or without contact) are:

$$\tau_{xz}^{aj}(x, z_{aj}) = \tau_{xz}^{aj}(x) = \tau_{aj} = 0; \tag{44}$$

$$\sigma_{zz}^{aj}(x, z_{aj}) = \frac{\beta_j\lambda E_{aj}(w_i - w_c)}{c_{aj}}; \tag{45}$$

where $\beta_j = \beta_j^c \cdot \beta_j^{frp}$.

Nonlinear governing equations. The nonlinear governing equations for the strengthened regions (fully bonded or debonded) are derived using Equations (12)–(20), the constitutive relations (Equations (34)–(39)), the compatibility requirements, Equations (7b), (9b) (in the bonded case), and the stress and deformation fields of the adhesive layers (Equations (40)–(45)). The governing equations are stated in terms of the unknown displacements and rotations, $(w_c, w_{\text{frp1}}, w_{\text{frp2}}, u_{oc}, u_{o\,\text{frp1}}, u_{o\,\text{frp2}}, \phi_c, \phi_{\text{frp1}}, \phi_{\text{frp2}})$,

and the unknown shear stresses (τ_{a1} and τ_{a2}), and read:

$$A_{11}^{\text{frp1}}\left(u_{o\,\text{frp1},xx}+w_{\text{frp1},x}w_{\text{frp1},xx}\right)-B_{11}^{\text{frp1}}\phi_{\text{frp1},xx}-\alpha_1^{frp}\alpha_1^c b_{\text{frp1}}\tau_{a1}=0; \tag{46}$$

$$A_{11}^{c}\left(u_{oc,xx}+w_{c,x}w_{c,xx}\right)-B_{11}^{c}\phi_{c,xx}-\alpha_2^{frp}\alpha_2^c b_{\text{frp2}}\tau_{a2}+\alpha_1^{frp}\alpha_1^c b_{\text{frp1}}\tau_{a1}=-n_x; \tag{47}$$

$$A_{11}^{\text{frp2}}\left(u_{o\,\text{frp2},xx}+w_{\text{frp2},x}w_{\text{frp2},xx}\right)-B_{11}^{\text{frp2}}\phi_{\text{frp2},xx}+\alpha_2^{frp}\alpha_2^c b_{\text{frp2}}\tau_{a2}=0; \tag{48}$$

$$A_{55}^{\text{frp1}}\left(w_{\text{frp1},xx}-\phi_{\text{frp1},x}\right)+A_{11}^{\text{frp1}}\left((w_{\text{frp1},x}u_{o\,\text{frp1},x}),_x+\frac{3}{2}w_{\text{frp1},xx}(w_{\text{frp1},x})^2\right)$$
$$-B_{11}^{\text{frp1}}\left(w_{\text{frp1},x}\phi_{\text{frp1},x}\right),_x+\frac{\alpha_1^{frp}\alpha_1^c b_{\text{frp1}}c_{a1}}{2}\tau_{a1,x}-\beta_1\frac{b_{\text{frp1}}E_{a1}}{c_{a1}}(w_{\text{frp1}}-w_c)=0; \tag{49}$$

$$A_{55}^{c}(w_{c,xx}-\phi_{c,x})+A_{11}^{c}\left((w_{c,x}u_{oc,x}),_x+\frac{3}{2}w_{c,xx}(w_{c,x})^2\right)$$
$$-B_{11}^{c}(w_{c,x}\phi_{c,x}),_x+\frac{\alpha_2^{frp}\alpha_2^c b_{\text{frp2}}c_{a2}}{2}\tau_{a2,x}+\frac{\alpha_1^{frp}\alpha_1^c b_{\text{frp1}}c_{a1}}{2}\tau_{a1,x}$$
$$+\beta_2\frac{b_{\text{frp2}}E_{a2}}{c_{a2}}(w_{\text{frp2}}-w_c)+\beta_1\frac{b_{\text{frp1}}E_{a1}}{c_{a1}}(w_{\text{frp1}}-w_c)=-q_z; \tag{50}$$

$$A_{55}^{\text{frp2}}(w_{\text{frp2},xx}-\phi_{\text{frp2},x})+A_{11}^{\text{frp2}}\left((w_{\text{frp2},x}u_{o\,\text{frp2},x}),_x+\frac{3}{2}w_{\text{frp2},xx}(w_{\text{frp2},x})^2\right)-B_{11}^{\text{frp2}}(w_{\text{frp2},x}\phi_{\text{frp2},x}),_x$$
$$+\alpha_2^{frp}\alpha_2^c b_{\text{frp2}}c_{a2}\tau_{a2,x}-\beta_2\frac{b_{\text{frp2}}E_{a2}}{c_{a2}}(w_{\text{frp2}}-w_c)=0; \tag{51}$$

$$D_{11}^{\text{frp1}}\phi_{\text{frp1},xx}-B_{11}^{\text{frp1}}\left(u_{o\,\text{frp1},xx}+w_{\text{frp1},x}w_{\text{frp1},xx}\right)+A_{55}^{\text{frp1}}(w_{\text{frp1},x}-\phi_{\text{frp1}})-\alpha_1^{frp}\alpha_1^c b_{\text{frp1}}\frac{d_{\text{frp1}}}{2}\tau_{a1}=0; \tag{52}$$

$$D_{11}^{c}\phi_{c,xx}-B_{11}^{c}\left(u_{oc,xx}+w_{c,x}w_{c,xx}\right)+A_{55}^{c}(w_{c,x}-\phi_c)-\alpha_2^{frp}\alpha_2^c b_{\text{frp2}}\frac{d_c}{2}\tau_{a2}-\alpha_1^{frp}\alpha_1^c b_{\text{frp1}}\frac{d_c}{2}\tau_{a1}=-m_y; \tag{53}$$

$$D_{11}^{\text{frp2}}\phi_{\text{frp2},xx}-B_{11}^{\text{frp2}}\left(u_{o\,\text{frp2},xx}+w_{\text{frp2},x}w_{\text{frp2},xx}\right)+A_{55}^{\text{frp2}}(w_{\text{frp2},x}-\phi_{\text{frp2}})-\alpha_2^{frp}\alpha_2^c b_{\text{frp2}}\frac{d_{\text{frp2}}}{2}\tau_{a2}=0; \tag{54}$$

$$\alpha_1^{frp}\alpha_1^c\left(u_{oc}-u_{o\,\text{frp1}}-\frac{c_{a1}}{2}(w_{\text{frp1},x}+w_{c,x})+\frac{\tau_{a1}c_{a1}}{G_{a1}}-\frac{\tau_{a1,xx}c_{a1}^3}{12E_{a1}}-\frac{d_{\text{frp1}}}{2}\phi_{\text{frp1}}-\frac{d_c}{2}\phi_c\right)=0; \tag{55}$$

$$\alpha_2^{frp}\alpha_2^c\left(u_{o\,\text{frp2}}-u_{oc}-\frac{c_{a2}}{2}(w_{\text{frp2},x}+w_{c,x})+\frac{\tau_{a2}c_{a2}}{G_{a2}}-\frac{\tau_{a2,xx}c_{a2}^3}{12E_{a2}}-\frac{d_{\text{frp2}}}{2}\phi_{\text{frp2}}-\frac{d_c}{2}\phi_c\right)=0. \tag{56}$$

In the debonded subregions, the shear stresses τ_{a1}, τ_{a2}, or both vanish. Correspondingly, Equation (55), Equation (56), or both, which result from the requirement of compatible longitudinal deformation, also vanish.

The nonlinear governing equations and the corresponding boundary and continuity conditions are numerically solved using the Nonlinear Multiple Shooting method [Stoer and Bulirsch 1993]. Along with the geometrical nonlinearity, the model is associated with further nonlinearities due to the unknown type of debonded subregions (with or without out-of-plane contact), and due to the cracking of the mortar joints. The determination of the type of debonded subregions is conducted iteratively. Namely, one type is assumed and verified through the results of the analysis. If the results contradict the assumption, the assumed type of the debonded region is switched and the structure is reanalyzed. The nonlinearity associated with the cracking of the mortar joints is considered through the following iterative procedure.

Step 1: initial guess. All mortar joints are assumed uncracked.

Step 2: analysis of the structure. Using the rigidities calculated in the initial guess or in the previous iteration, the nonlinear governing equations are numerically solved using the multiple shooting method [Stoer and Bulirsch 1993].

Step 3: analysis of the mortar joints cross-section. Based on the solution obtained in Step 2, the location of the cracked mortar joints and the depth of the compression zone in each cracked joint are determined as follows.

(i) The strain distribution in each mortar joint is determined through Equation (3a). If the maximum tensile strain plus the initial compressive strain due to the self-weight exceeds the ultimate tensile/bond strain of the mortar, the joint is considered cracked.

(ii) In each cracked joint, the depth of the active zone is determined as:

$$z_{act}^{\mathrm{mj}} = \frac{u_{o\,\mathrm{mj},x} + \frac{1}{2}(w_{\mathrm{mj},x})^2}{\phi_{\mathrm{mj},x}} - \frac{\varepsilon_t^{\mathrm{mj}}}{\phi_{\mathrm{mj},x}}; \tag{57}$$

where $u_{o\,\mathrm{mj},x}$, $w_{mj,x}$ and $\phi_{\mathrm{mj},x}$ are obtained in Step 2.

(iii) Once z_{act}^{mj} is determined, the rigidities of each joint are evaluated using Equations (38)a–d. Due to the relatively small height of the joints (with respect to the height of the wall), it is assumed that the rigidities are uniform through the height of each joint.

Step 4: convergence criterion. If the norm of the relative difference between the magnitudes of the equivalent rigidities of the mortar joints in two successive iterations is sufficiently small, the iterative procedure is stopped. Otherwise, the procedure returns to Step 2 with the updated rigidities determined in Step 3.

Numerical study

The numerical study focuses on the geometrically nonlinear effects in the bending behavior of a masonry wall strengthened with externally bonded FRP strips. In many practical cases, masonry walls are strengthened to carry sign-reversing loads and the FRP strengthening system is applied on both faces of the wall. This type of strengthening scheme is examined as follows. The geometry of the wall, the strengthening scheme, the mechanical properties of the materials, and the static load pattern appear in Figure 4. The FRP strips are assumed to be fully bonded in the uncracked stage. However, once the joint is cracked, it is assumed that the crack opening, the extensive longitudinal strains in the FRP strip bridging over the crack, and the inability of the cracked faces to transfer shear stresses trigger the formation of a debonded region along the cracked joint. Studies on externally strengthened concrete beams [Rabinovitch and Frostig 2000; Rabinovitch and Frostig 2001; Teng et al. 2002] and preceding studies on the geometrically linear response of strengthened masonry walls [Hamed and Rabinovitch 2005] revealed that the characteristic length scale of the peeling stress concentrations near the edge of the FRP strip, near cracks, or near the mortar joint is about the thickness of the adhesive layer. (The peeling stress concentration decays within a distance of about 2 to 3 times the thickness of the adhesive

layer). Hence, it is assumed that the height of each debonded region equals the height of the mortar joint plus twice the thickness of the adhesive layer (Figure 4d). In order to examine the role of the assumed height of the debonded region, the influence of this parameter is parametrically studied over a range of zero to three times the thickness of the adhesive layer. The effect of the existence of debonded regions in *all* mortar joints, which may result from imperfect placement of the adhesive or from preloading of the strengthened wall, is also investigated. Finally, the effect of the slenderness ratio is examined.

The load-deflection curves (equilibrium paths) and the in-plane thrust force (the *arching force*) versus the out-of-plane deflection curves of the strengthened and the unstrengthened masonry walls appear in Figure 5. In order to highlight the geometrically nonlinear effects, the results of a geometrically linear, but physically nonlinear (cracking) analysis of the strengthened wall also appear in Figure 5. The results show that both the unstrengthened wall and the strengthened wall are characterized by a limit point and a snap-through type of behavior [Simitses 1986]. Due to the ability of the strengthened wall to carry bending moments through tensile stresses in the FRP strip and compressive stresses in the masonry panel, the post-limit-point slope of the equilibrium path and the magnitudes of the arching force in the strengthened wall are lower than those in the unstrengthened one (see Figure 5b). The latter observation is in qualitative agreement with the experimental findings of [Galati et al. 2002], which revealed a reduction in the magnitude of the thrust force with the increase of the width (and cross sectional area) of the

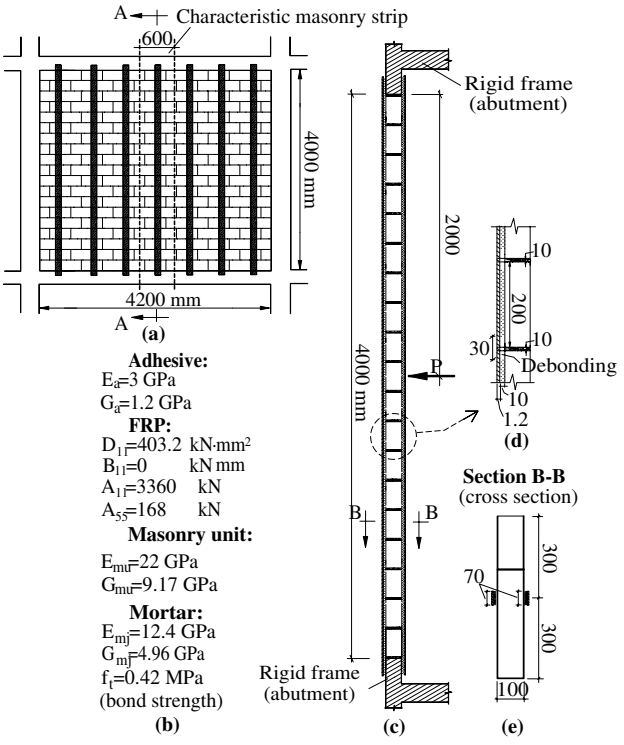

Figure 4. Geometry, material properties, and loading: (a) geometry; (b) material properties; (c) section A-A: geometry and loading; (d) cracked mortar joint and debonded regions; (e) section B-B (cross section).

strengthening system. The comparison between the nonlinear results and the linear ones clearly indicates that the decrease in the overall flexural rigidity of the strengthened wall along its equilibrium path results from the destabilizing nonlinear effects of the arching action, and not from the progressive cracking of the mortar joints. Note that the load-deflection curve in the geometrically linear case is almost linear due to the early cracking of the mortar joints under very low load levels.

In quantitative terms, Figure 5a shows that the limit point load and deflection of the unstrengthened masonry wall are about 25.4 kN and 40 mm, respectively, while those of the strengthened wall are about 36 kN and 55.5 mm, respectively. Thus, the use of the bonded FRP strips improves the stability characteristics of the wall (both the limit point load and the limit point deflection) by a factor of about 1.4. A similar *improvement factor* of the limit point load was detected in the experimental study of [Tumialan et al. 2003]. Yet, this value is much smaller than the factors experimentally detected for strengthened simply supported and longitudinally unconstrained walls [Gilstrap and Dolan 1998; Albert et al. 2001; Hamilton and Dolan 2001; Hamoush et al. 2002].

The response of the strengthened and the unstrengthened masonry walls under a displacement level of 20 mm at midspan and load levels of about 24 kN and 20 kN, respectively, is studied in Figure 6. The out-of-plane and the in-plane deflections appear in Figure 6 a,b. These figures reveal that due to the progressive cracking of the critical mortar joints at the edges and at midspan, the deformation of the wall is governed by a system of three hinged rigid bodies. A level of elastic curvature, which is slightly more prominent in the strengthened wall, is also observed due to localized bending of the masonry units (Figure 6a). Figure 6b further reveals the *jumps* in the distribution of the longitudinal deformations due to cracking of the critical joints. The distributions of the bending moments, the in-plane forces, and the shear forces appear in Figures 6c–e, respectively, and reveal the localized effects in the vicinity of the cracked mortar joints. These effects result from the prominent change in stiffness between the masonry unit section and the cracked mortar joint section. In the masonry unit section, the considerable flexural stiffness of the masonry unit allows a larger portion of the global bending moment to be carried by the masonry unit itself. As a result, the part of the global moment carried in the form of tensile forces in the

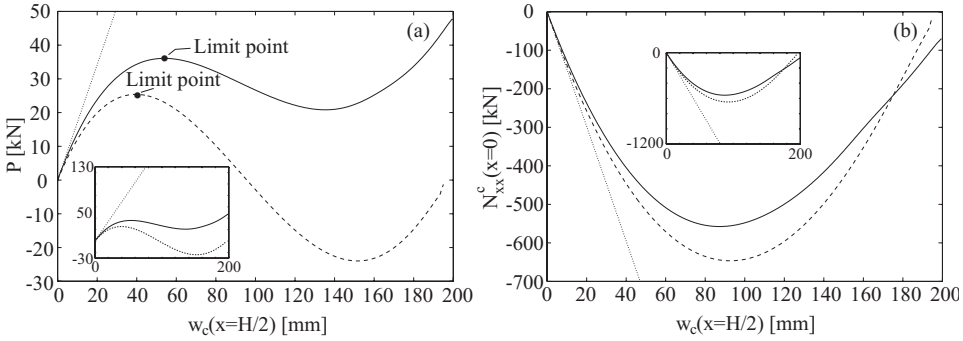

Figure 5. Response of strengthened and unstrengthened masonry wall: (a) equilibrium paths (load versus deflection); (b) "thrust force" versus deflection. (Legend: — strengthened wall (nonlinear analysis); - - - unstrengthened wall (nonlinear analysis); ··· strengthened wall (linear analysis).)

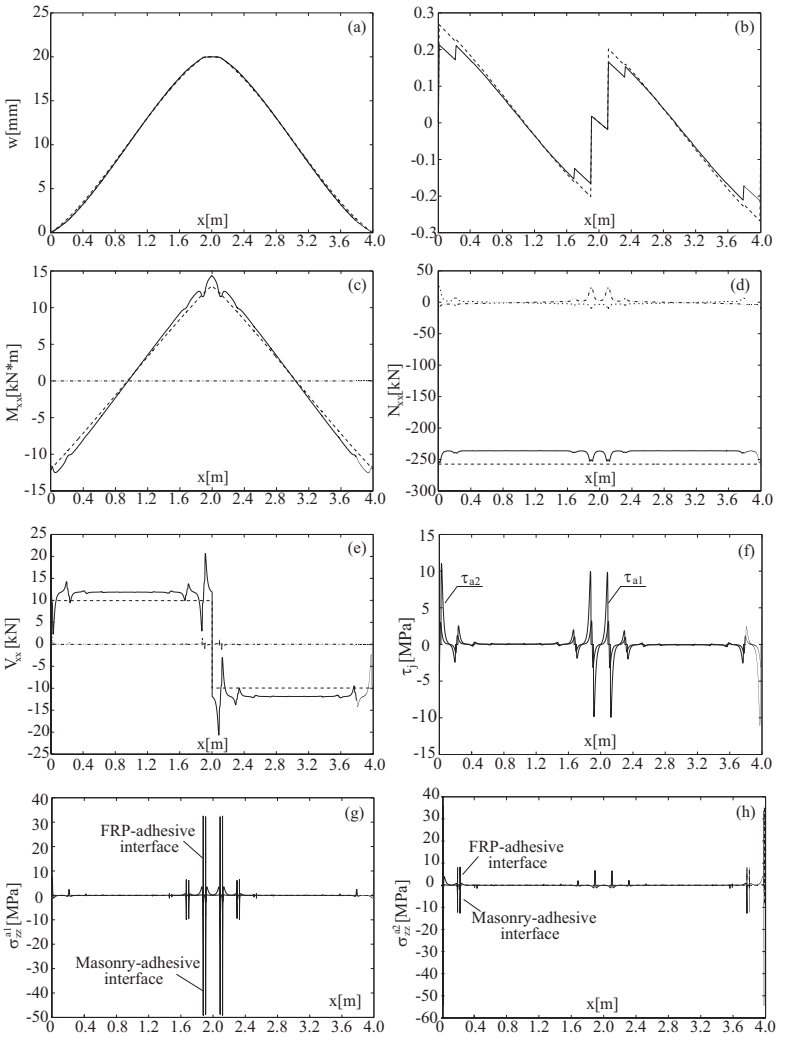

Figure 6. Response under midspan displacement of 20 mm: (a) out-of-plane deflections; (b) in-plane deformations; (c) bending moments; (d) axial forces; (e) shear forces; (f) adhesive shear stresses; (g) out-of-plane normal stresses, inner adhesive layer; (h) out-of-plane normal stresses, outer adhesive layer. (Legend: — strengthened wall; - - - unstrengthened wall; -·-·- inner FRP strip; · · · outer FRP strip).

FRP strip and compressive force in the wall (the *composite action* moment) is much smaller than in the cracked mortar joint section. The variation of the tensile force in the FRP strip from the cracked joint section to the masonry unit section yields the shear stress concentrations observed in Figure 6f. Figures 6d and 6e also reveal locally increased shear and compressive forces in the masonry panel. These effects

may lead to the shear-compression crushing failure experimentally observed by Tumialan et al., [2000; 2003] and Galati et al. [2002].

The localized effects near the cracked joints and especially the rapid variation in the shear stresses (Figure 6f) also trigger the development of out-of-plane normal (peeling) stress concentrations (see Figures 6g, 6h and Equation (41)). Note that in the inner adhesive layer, the stress concentrations develop due to crack opening at the inner face of the mortar joints near midspan. In the outer adhesive layer, they develop due to crack opening at the outer face of the edge joints. These stress concentrations quantify and explain the debonding mechanisms experimentally observed by Hamilton and Dolan [2001], Carney and Myers [2005] and others.

Effect of debonded regions and local buckling. In many cases, the development of debonded regions is not limited to the vicinity of the cracked joints, but may also form due to imperfect placement of the adhesive or to preloading of the strengthened wall. The influence of the existence of debonded regions near all mortar joints is studied in Figure 7. Figure 7a shows that the overall equilibrium path (load-deflection curve) of the strengthened wall is only slightly affected by the existence of the debonded regions near all mortar joints (as compared to the case debonded regions are formed near the cracked joints only). On the other hand, the response in terms of the longitudinal normal stresses at the inner and outer faces of the compressed FRP strip near midspan (Figure 7b) reveals significant differences between

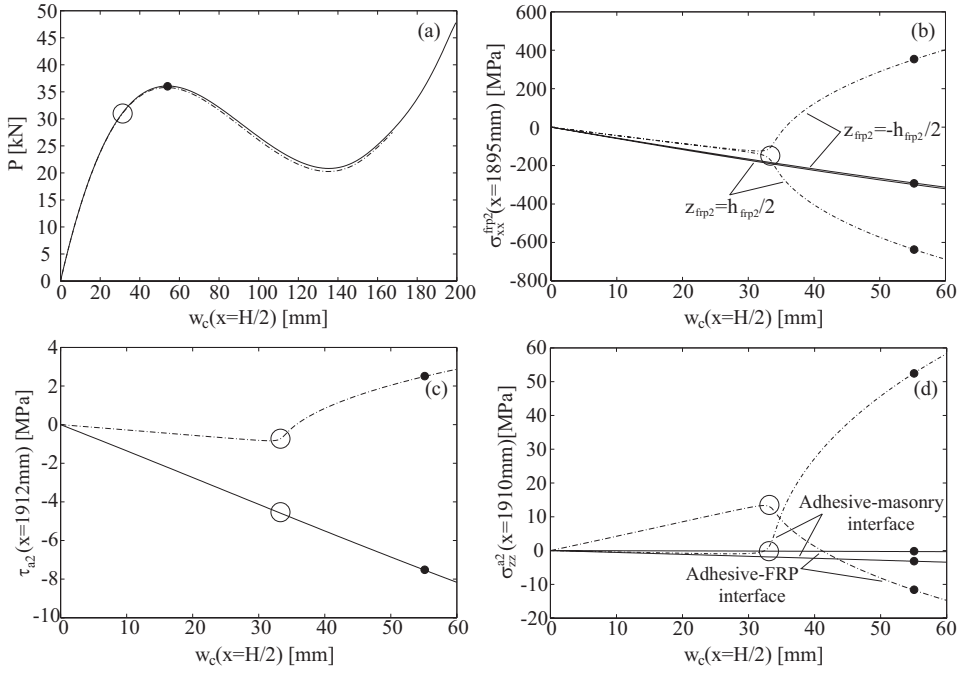

Figure 7. Equilibrium paths and stresses in the FRP strip and the adhesive versus midspan deflection: (a) equilibrium paths; (b) longitudinal stresses in the outer FRP strip; (c) shear stresses in the adhesive; (d) out-of-plane normal stresses in the adhesive. (Legend: — debonding in the cracked joints only; -·-·- debonding in all joints; • limit point; ∘ wrinkling).

the two cases. In case the FRP strip is fully bonded, the two faces are subjected to an almost equal level of compressive stresses, and the effect of the local bending moment is minor. In the debonded case, starting from a load level of about 31.3 kN (and a displacement level of about 32 mm), the local bending moment significantly affects the in-plane normal stresses. This bending moment is a direct result of the local buckling (wrinkling) of the compressed FRP.

The effect of the localized buckling and wrinkling phenomena on the shear and the out-of-plane normal stresses in the adhesive at the edges of the debonded region near midspan is studied in Figures 7c and 7d, respectively. These curves show that once the compressed FRP has buckled, the shear stresses and, particularly, the out-of-plane normal stresses are significantly increased. Furthermore, while the adhesive-masonry interface is in compression in the prebuckling stage, beyond the local buckling point it is subjected to tensile stresses. Due to the brittleness and the low out-of-plane tensile strength of the masonry material, this may trigger the growth of the debonded region, and may lead to total failure of the strengthening system. The results presented here in terms of stress fields in relation to this effect can be used for the quantitative evaluation of a fracture-mechanics based criterion for the growth of the debonded regions [Rabinovitch and Frostig 2001; 2006; Rabinovitch 2004a]. The results also show that the local buckling of the FRP strip occurs at a load level that is lower than the limit point load. Hence, in this case, the localized stability effects are expected to be more dominant than the global ones.

The out-of-plane deflections and the in-plane normal stresses in the FRP strip under load levels of 28.5 kN and 33.5 kN appear in Figure 8 and clearly show the wrinkling of the FRP strip within the debonded region (Figure 8a). Figure 8b reveals the considerable amplification of the in-plane normal stresses in the inner and outer faces of the FRP strip. Also there, is the direct result of the bending moments that develop due to the local buckling of the FRP strips.

Effect of the height of the debonded regions (h_{deb}). The influence of the height of debonded regions on the local and global behavior of the strengthened wall (in case debonded regions are formed near all joints) is parametrically studied in Figure 9. The results show that the height of the debonded regions does not qualitatively affect the general pattern of the nonlinear behavior of the strengthened wall. However, Figures 9 a, c, d show that the limit point loads and the limit point displacements detected with very

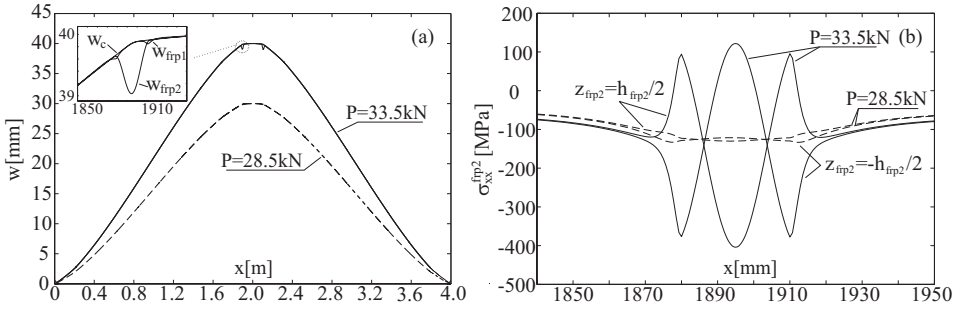

Figure 8. Response of the strengthened wall with debonded regions in all joints: (a) out-of-plane deflections along the wall; (b) longitudinal stresses in the faces of the outer FRP strip. (Legend: — response under $P = 33.5$ kN ($w_{c,\max} = 40$ mm); - - - response under $P = 28.5$ kN ($w_{c,\max} = 30$ mm)).

short debonded regions ($h_{deb} \to 0$) are notably higher than the ones detected with the higher (up to 70 mm) ones. In other words, the results show that the height of the debonded regions affects the limit point load and the limit point deflection *improvement factors* of the strengthening system (that is, the ratios of the limit point load or deflection of the strengthened wall over those of the original wall). These factors range from about 1.65 for the short debonded regions to only about 1.2 for the longer debonded regions. Figures 9b and 9d further show that, as expected, the magnitudes of the wrinkling load of the compressed FRP strip significantly decrease with the increase of the height of the debonded regions. Note that in the case of debonded region shorter than 20 mm, wrinkling of the FRP strip does not occur. The results observed in Figure 9 clarify that the height of the debonded region quantitatively affects the global nonlinear behavior of the wall and critically governs the localized response (wrinkling) near the cracked joint. Furthermore, the results highlight the necessity of a fracture mechanics approach to the debonding growth mechanism [Rabinovitch and Frostig 2001; 2006; Rabinovitch 2004a]. This approach can be applied based on the stress and displacement fields detected here.

Effect of the slenderness ratio. Four strengthened URM walls with different slenderness ratios, ($H/h_c =$ 21.1, 31.6, 40, and 52.6) are examined. The dimensions of the masonry units and the mortar joints are the same for all walls, while the slenderness ratio is controlled by modifying the number of the masonry units. The *normalized* load-deflection curves (equilibrium paths) for the four unstrengthened walls, the

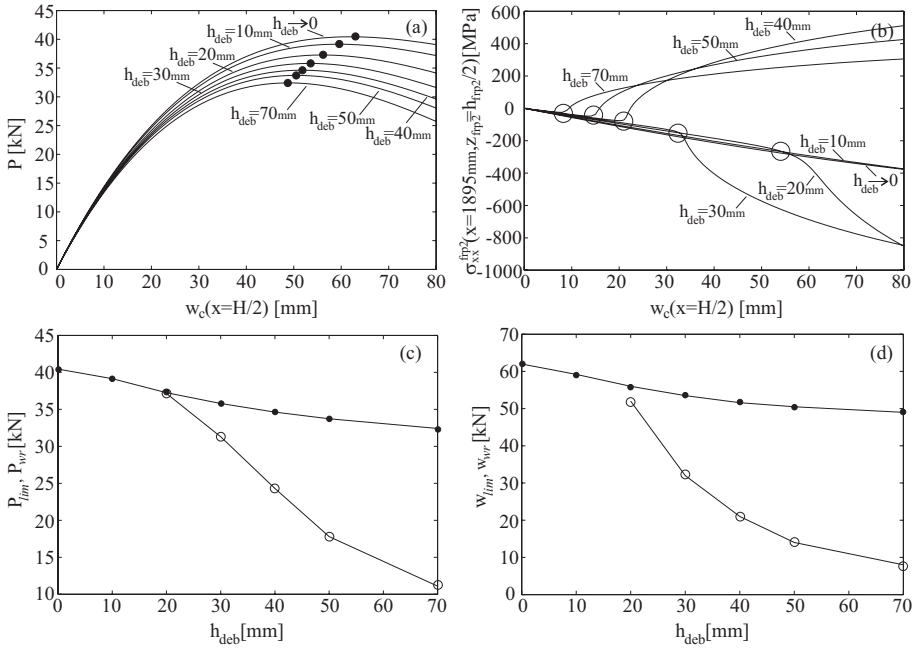

Figure 9. Influence of the height of debonded regions (h_{deb}): (a) equilibrium paths; (b) longitudinal stresses in the outer FRP strip; (c) critical (limit point, winkling) load versus h_{deb}; (d) critical (limit point, winkling) displacement versus h_{deb}. (Legend: • limit point; ○ wrinkling point).

strengthened walls with debonded regions near the cracked joints only, and the strengthened walls with debonded regions near all joints appear in Figure 10. (Note that in some cases, numerical convergence was not achieved and the deep post-limit-point response, which is of less practical importance, was not detected). The *normalized* results show that walls with different slenderness ratios exhibit a qualitatively similar nonlinear behavior with a limit point and a snap through. Considering the *limit point load improvement factor* of the strengthening system it is seen that for the configuration studied here (with $h_{deb} = 30\,\text{mm}$), this normalized factor is about 1.4 for all slenderness ratios. The results further show that the strengthening system modifies the limit point deflection and increases it from about $0.4h_c$ in the unstrengthened walls to about $0.55h_c$ in the strengthened ones. Also, the *limit point deflection improvement factor* equals about 1.4 for all slenderness ratios.

In quantitative terms, the critical limit point load drops down from 223 kN in the strengthened stubby wall to about 29 kN in the most slender one. Yet, the critical limit point deflection is about 55 mm in all cases. The reduction in the critical load (limit point loads, P_{lim}, or wrinkling load, P_{wr}) with the increase of the slenderness ratio is quantitatively studied in Figure 11. These results emphasize that in the high slenderness ratios ($H/h_c = 40, 52.6$), the geometrically destabilizing effects may lead to loss of stability before exceeding the ultimate strength of the materials [Carney and Myers 2005]. The ability to explore and quantify these geometrically nonlinear effects is essential for the design and use of the strengthened wall.

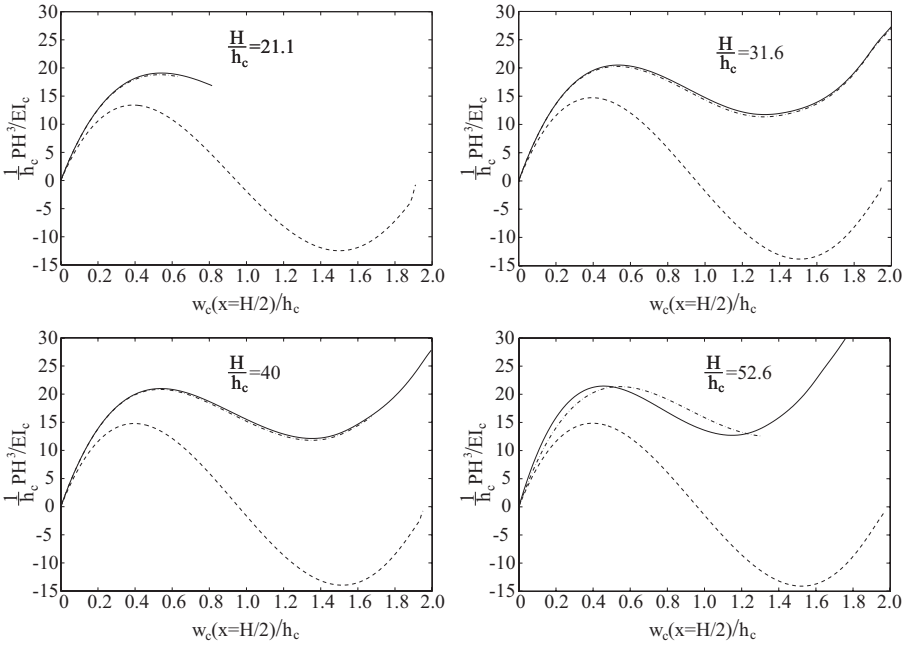

Figure 10. Normalized equilibrium paths for different slenderness ratios. (Legend: — strengthened wall with debonded regions near the cracked joints only; -·-·- strengthened wall with debonded regions near all joints; - - - unstrengthened wall).

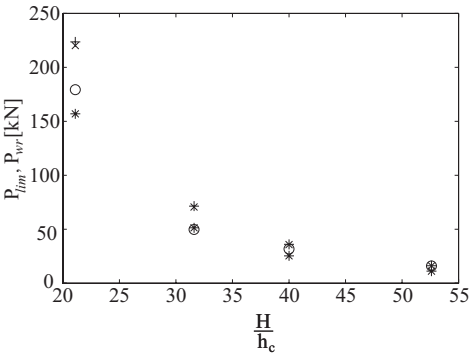

Figure 11. Critical loads (limit point load, wrinkling load) versus slenderness ratio. (Legend: $*$ unstrengthened wall limit point; $+$ strengthened wall limit point; $\cdot$ strengthened wall with debonded regions in all joints—limit point; $\circ$ wrinkling load).

Comparison to finite element analysis

In this section, the results obtained through the nonlinear theoretical model developed here are compared to finite element analysis (FEA), using the commercial package ANSYS. The geometry of two blocks specimen, the mechanical properties of the materials, and the 2D finite element model appear in Figure 12. The analytical model assumes that debonded regions develop at the mortar joints in case of imperfect placement of the adhesive, or in case of cracking of the joint. Correspondingly, the same assumption

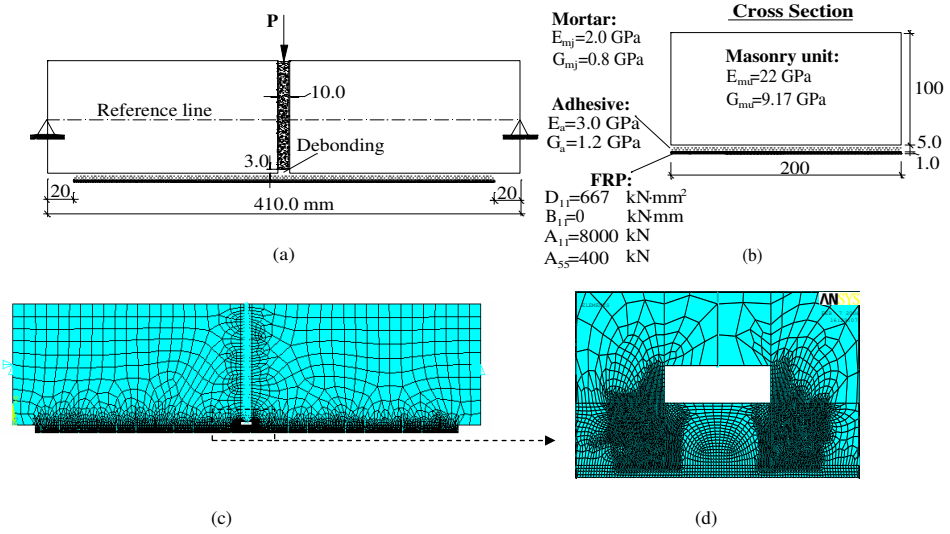

Figure 12. Geometry, material properties, and load pattern for masonry specimens: (a) geometry and load; (b) cross section and material properties; (c) finite element mesh; (d) zoom on the mortar joint.

is made in the FE model and a 3.0 mm deep and 10.0 mm high gap is assumed between the mortar and the adhesive (see Figure 12a). The nonlinear effect of mortar joint cracking is considered as a contact problem, using contact and target surface elements located at midspan. The masonry, the mortar, the FRP strip, and the adhesive are modeled using 4 node elements, and they are assumed to be linear elastic. Yet, due to the extensive longitudinal strains and the probable cracking or yielding of the adhesive fillet that is attached to the debonded FRP strip within the cracked mortar joint, it is assumed that its longitudinal rigidity is significantly smaller than its out-of-plane normal rigidity. The number of elements used through the thin adhesive layer varies from 5 to 15 at the critical locations. The number of elements used through the thickness of the FRP strip is 4, and the number of elements through the depth of the masonry block is about 15. The total number of elements used in the nonlinear FEA of the two masonry units specimen is as large as 21588. This huge number of elements is required, due to the different length scales of the structure components and due to the singular points near the debonded region and near the edges of the FRP strip (also see the FE model in [Davidson et al. 2005]). Two point supports that restrict the longitudinal and the vertical displacements are located at the edges of the specimen at midheight.

The nonlinear equilibrium paths of the strengthened and the unstrengthened specimens obtained by the theoretical and the FE models appear in Figure 13. The results reveal fair agreement between the numerical and the theoretical curves. In the strengthened wall, good agreement is observed at relatively low and medium load levels. Under higher loads, the results of the FE model deviate from the equilibrium path obtained by the theoretical model. This is mainly attributed to the localized effects observed near the supports in the FE model (stress concentrations and localized deformations), and the different modeling of the cracking at the mortar joint (critical section cracking in the FE model compared with cracking of the entire length of the mortar joint in the theoretical model). The different modeling of the effect of shear deformation (first order beam theory versus 2D elasticity) may also contribute to the differences observed; however, this effect is probably secondary to other contributing factors mentioned above. Figure 13 also shows that the theoretical model predicts the limit point behavior of the strengthened masonry specimen, whereas the FE model diverges under a displacement level that is 3% higher than the limit

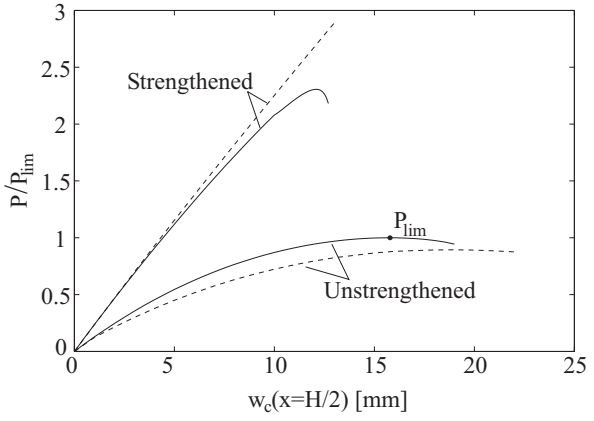

Figure 13. Equilibrium paths of strengthened and unstrengthened specimens. (Legend: — theoretical model; - - - FE model).

point displacement predicted by the theoretical model. At that point, the load predicted by the FE model is about 25% higher than the limit point load determined by the theoretical model. In the unstrengthened wall, the FE model succeeds in describing the limit point behavior and predicts a limit point load that is about 10% lower than the one predicted by the theoretical model.

The distributions of the normalized axial force in the FRP strip and the shear and peeling stresses in the adhesive are described in Figure 14. It is seen that the results of the FE analysis and those of the theoretical model are in good agreement. Figure 14a shows that the FEA also predicts that the axial force in the FRP strip is almost constant through the length of the debonded region at the mortar joint. This is due to the negligible shear stresses in the adhesive within the debonded region (Figure 14b). In the theoretical model these stresses totally vanish (Figure 14b), and the axial force in the FRP strip is uniform within the debonded region (Figure 14a). The distribution of the peeling stresses at the interfaces of the adhesive layer near the cracked mortar joint appears in Figure 14c, and also reveals an impressive agreement between the numerical and the theoretical models.

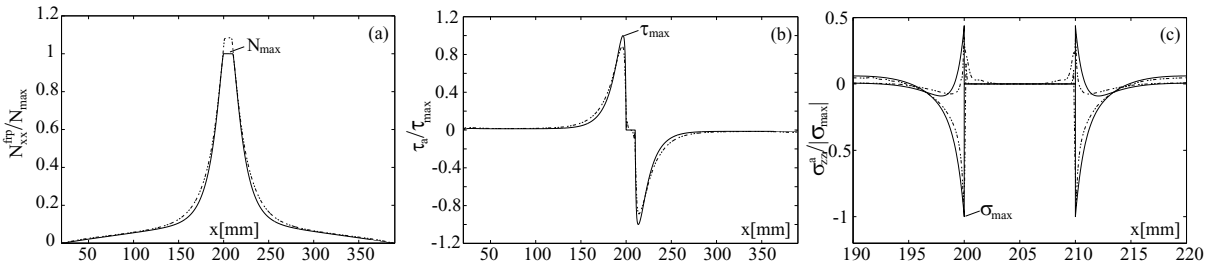

Figure 14. Response of the strengthened masonry specimen under a midspan displacement of 4 mm: (a) normalized axial forces in the FRP; (b) shear stresses in the adhesive; (c) peeling stresses in the adhesive near the joint. (Legend: — theoretical model; - - - FE model).

Opposed to the analytical stress fields used in the theoretical model (Equations (40)–(45)), the FEA is strongly affected by the singular character of the stresses near the edges of the debonded region. As a result, it is sensitive to the mesh characteristics in this region. The convergence of the FE peak shear and normal stresses in the adhesive, with the refinement of the mesh, is studied in Figure 15 (note that in both analyses, the same debonded region is assumed). The results are normalized and the ratios of the peak stresses computed by the FE model (τ_{FE} and $\sigma_{\mathrm{FE}}^{zz}$) over the peak stresses obtained by the theoretical model (τ_{Th} and $\sigma_{\mathrm{Th}}^{zz}$) are presented. The results in Figure 15 indicate that the numerical FE results converge towards the theoretical values with the refinement of the mesh. This trend is most notable in terms of the peak normal stresses, which are more affected by the singularity at the edges of the debonded region. This observation indicates that for cases in which the mesh of the FE model is not as fine as required, the FE model could underestimate the critical stresses in the adhesive. Due to the critical importance of theses stresses, the results presented here highlight one of the most problematic aspects of the FEA of the strengthened wall and emphasize the advantages of the theoretical model.

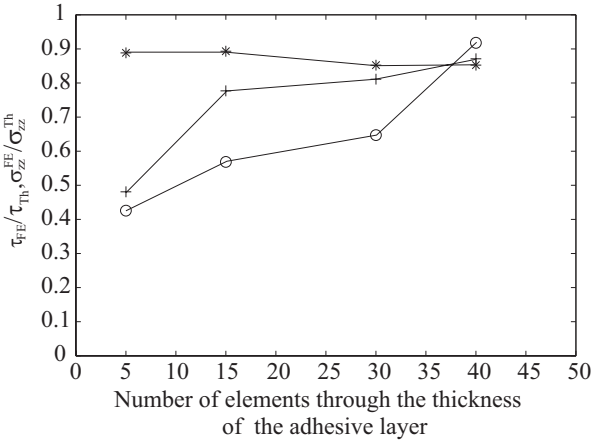

Figure 15. Convergence of the peak shear and peeling stresses near the mortar joint with mesh refinement. (Legend: $*$ shear stresses; $+$ peeling stresses at the adhesive-FRP interface; $\circ$ peeling stresses at the adhesive-masonry interface).

Concluding remarks

The geometrically nonlinear effects of the out-of-plane flexural response of URM walls strengthened with composite materials have been investigated. A general theoretical approach and a nonlinear analytical model for the geometrically nonlinear analysis of the strengthened masonry wall have been presented. The analytical model and the numerical study have revealed a global limit-point and snap-through type of behavior that is governed by the destabilizing influence of the arching action as well as localized wrinkling effects in the compressed FRP strip. The results have also shown that the use of the bonded FRP system can potentially improve the global stability characteristics of the wall and increases its limit point load and deflection by a factor of 1.2–1.65.

The effect of the formation of debonded regions in the vicinity of the mortar joints has been examined. It has been shown that the formation of debonded regions promotes the development of wrinkling or local buckling of the compressed FRP strip. This phenomenon significantly magnifies the normal stresses in the FRP strip as well as the shear and peeling stresses in the adhesive. Thus, it may trigger an overall debonding failure of the strengthening system. In addition, it has been quantitatively shown that the increase in the height of the debonded regions affects the global nonlinear behavior of the strengthened wall and reduces the magnitude of the local wrinkling load as well as the effectiveness of the strengthening system.

The study of the influence of the slenderness ratio has shown that strengthened walls of different slenderness ratios exhibit a qualitatively similar nonlinear behavior. Quantitatively, the investigation has characterized the reduction in the global limit point load with the increase of the slenderness ratio and has highlighted the role of the geometrically nonlinear effects in the response of the slender strengthened walls.

In conclusion, the analytical model and the numerical study presented have shed some light on the global (limit-point and snap through behavior) and localized (wrinkling) geometrically nonlinear effects

in the out-of-plane behavior of URM walls strengthened with composite materials. Due to their critical influence on the structural response of the strengthened wall, these geometrically and physically nonlinear effects must be carefully considered in order to assure the effective design and the safe use of the strengthened wall.

References

[Albert et al. 2001] M. L. Albert, A. E. Elwi, and J. J. R. Cheng, "Strengthening of unreinforced masonry walls using FRPs", *J. Compos. Constr.* **5**:2 (2001), 76–84.

[Anderson 1984] C. Anderson, "Arching action in transverse laterally loaded masonry wall panels", *The Structural Engineer* **62B**:1 (1984), 12–23.

[Carney and Myers 2005] P. Carney and J. J. Myers, "Out-of-plane static and blast resistance of unreinforced masonry wall connections strengthened with FRP", pp. 229–248 in *Fiber-reinforced polymer (FRP) reinforcement for concrete structures: 7th international symposium* (Kansas City, MO, 2005), edited by C. K. Shield et al., American Concrete Institute, Farmington Hills, MI, 2005.

[Dafnis et al. 2002] A. Dafnis, H. Kolsch, and H. Reimerdes, "Arching in masonry walls subjected to earthquake motions", *J. Struct. Eng.* **128**:2 (2002), 153–159.

[Davidson et al. 2005] J. S. Davidson, J. W. Fisher, M. I. Hammons, J. R. Porter, and R. J. Dinan, "Failure mechanisms of polymer-reinforced concrete masonry walls subjected to blast", *J. Struct. Eng.* **131**:8 (2005), 1194–1205.

[Deuring 1993] M. Deuring, "Verstärken von Stahlbeton mit gespannten Faserverbundwerstoffen", EMPA Research report 224, Swiss federal laboratories for material testing and research, Dübendorf, 1993.

[Galati et al. 2002] N. Galati, J. G. Tumialan, A. La Tegola, and A. Nanni, "Influence of arching mechanism in masonry walls strengthened with FRP laminates", in *Third international conference on composites in infrastructure*, San Francisco, 2002.

[Ghobarah and El Mandooh Galal 2004] A. Ghobarah and K. El Mandooh Galal, "Out-of-plane strengthening of unreinforced masonry walls with openings", *J. Compos. Constr.* **8**:4 (2004), 298–305.

[Gilstrap and Dolan 1998] J. M. Gilstrap and C. W. Dolan, "Out-of-plane bending of FRP-reinforced masonry walls", *Compos. Sci. Technol.* **58**:8 (1998), 1277–1284.

[Griffith et al. 2004] M. C. Griffith, N. T. K. Lam, J. L. Wilson, and K. Doherty, "Experimental investigation of unreinforced brick masonry walls in flexure", *J. Struct. Eng.* **130**:3 (2004), 423–432.

[Hamed and Rabinovitch 2005] E. Hamed and O. Rabinovitch, "Out-of-plane bending of URM walls strengthened with FRP strips — modeling and analysis", pp. 249–268 in *Proceedings of the* 7^{th} *international symposium on fiber reinforced polymer (FRP) reinforcement for concrete structures*, edited by C. K. Shield et al., Kansas City, MO., November 6–9 2005.

[Hamilton and Dolan 2001] H. R. Hamilton and C. W. Dolan, "Flexural capacity of glass FRP strengthened concrete masonry walls", *J. Compos. Constr.* **5**:3 (2001), 170–178.

[Hamoush et al. 2002] S. A. Hamoush, M. W. McGinley, P. Mlakar, and M. J. Terro, "Out-of-plane behavior of surface-reinforced masonry walls", *Constr. Build. Mater.* **16**:6 (2002), 341–351.

[Hasetline and Moore 1981] B. A. Hasetline and J. F. A. Moore, *Handbook to BS5628: structural use of masonry, 1: unreinforced masonry*, Brick Development Association, Windsor, UK, 1981.

[Kiss et al. 2002] R. M. Kiss, L. P. Kollar, J. Jai, and H. Krawinkler, "Masonry strengthened with FRP subjected to combined bending and compression, II: test results and model predictions", *J. Compos. Mater.* **36**:9 (2002), 1049–1063.

[Kuzik et al. 2003] M. D. Kuzik, A. E. Elwi, and J. J. R. Cheng, "Cyclic flexure tests of masonry walls reinforced with glass fiber reinforced polymer sheets", *J. Compos. Constr.* **7**:1 (2003), 20–30.

[McDowell et al. 1956] E. L. McDowell, K. E. Mckee, and E. Sevin, "Arching action theory of masonry walls", *J. Struct. Div.* **82**:ST2 (1956), 915–1: 915–18.

[Rabinovitch 2004a] O. Rabinovitch, "Fracture-mechanics failure criteria for RC beams strengthened with FRP strips – a simplified approach", *Compos. Struct.* **64**:3–4 (2004), 479–492.

[Rabinovitch 2004b] O. Rabinovitch, "Nonlinear (buckling) effects in RC beams strengthened with composite materials subjected to compression", *Int. J. Solids Struct.* **41**:20 (2004), 5677–5695.

[Rabinovitch 2005] O. Rabinovitch, "Bending behavior of reinforced concrete beams strengthened with composite materials using inelastic and nonlinear adhesives", *J. Struct. Eng.* **131**:10 (2005), 1580–1592.

[Rabinovitch and Frostig 2000] O. Rabinovitch and Y. Frostig, "Closed-form high-order analysis of RC beams strengthened with FRP strips", *J. Compos. Constr.* **4**:2 (2000), 65–74.

[Rabinovitch and Frostig 2001] O. Rabinovitch and Y. Frostig, "Delamination failure of RC beams strengthened with FRP strips — a closed-form high-order and fracture mechanics approach", *J. Eng. Mech.* **127**:8 (2001), 852–861.

[Rabinovitch and Frostig 2006] O. Rabinovitch and Y. Frostig, "Fracture mechanics approach to geometrically nonlinear debonding problems in RC beams strengthened with composite materials", *Adv. Struct. Eng.* **9**:6 (2006), 765–777.

[Sheinman and Adan 1987] I. Sheinman and M. Adan, "The effect of shear deformation on post-buckling behavior of laminated beams", *J. Appl. Mech.* (*Trans. ASME*) **54**:3 (1987), 558–562.

[Simitses 1986] G. J. Simitses, *An introduction to the elastic stability of structures*, Krieger, Malabar, FL, 1986.

[Stoer and Bulirsch 1993] J. Stoer and R. Bulirsch, *Introduction to numerical analysis*, Springer, New York, 1993.

[Tan and Patoary 2004] K. H. Tan and M. K. H. Patoary, "Strengthening of masonry walls against out-of-plane loads using fiber-reinforced polymer reinforcement", *J. Compos. Constr.* **8**:1 (2004), 79–87.

[Teng et al. 2002] J. G. Teng, J. W. Zhang, and S. T. Smith, "Interfacial stresses in reinforced concrete beams bonded with a soffit plate: a finite element study", *Constr. Build. Mater.* **16**:1 (2002), 1–14.

[Timoshenko and Goodier 1970] S. Timoshenko and J. N. Goodier, *Theory of elasticity*, 3rd ed., McGraw-Hill, New York, 1970.

[Tumialan et al. 2000] G. Tumialan, D. Tinazzi, J. J. Myers, and A. Nanni, "Field evaluation of unreinforced masonry walls strengthened with FRP composites subjected to out-of-plane loading", in *ASCE Structures Congress*, edited by M. Elgaaly, Philadelphia, 2000. CD version.

[Tumialan et al. 2003] J. G. Tumialan, N. Galati, and A. Nanni, "Field assessment of unreinforced masonry walls strengthened with fiber reinforced polymer laminates", *J. Struct. Eng.* **129**:8 (2003), 1047–1056.

[UBC 1991] UBC, *Uniform building code*, International conference of building officials, Whittier, CA, 1991.

[Velazquez-Dimas et al. 2000] J. I. Velazquez-Dimas, M. R. Ehsani, and H. Saadatmanesh, "Out-of-plane behavior of brick masonry walls strengthened with fiber composites", *ACI Struct. J.* **97**:3 (2000), 377–387.

[Vinson and Sierakowski 1986] J. R. Vinson and R. L. Sierakowski, *The behavior of structures composed of composite materials*, Martinus-Nijhoff, Dordrecht, 1986.

Received 3 Apr 2006. Accepted 23 Sep 2006.

EHAB HAMED: ehab@tx.technion.ac.il
Faculty of Civil and Environmental Engineering, Technion — Israel Institute of Technology, Technion City, Haifa 32000, Israel

ODED RABINOVITCH: cvoded@tx.technion.ac.il
Faculty of Civil and Environmental Engineering, Technion — Israel Institute of Technology, Technion City, Haifa 32000, Israel